ARTICLES
PUBLISHED ONLINE: 16 FEBRUARY 2014 | DOI: 10.1038/NMAT3864
nature materials

Engineered materials for all-optical helicity-dependent magnetic switching

S. Mangin[1,2*], M. Gottwald[1], C-H. Lambert[1,2], D. Steil[3], V. Uhlíř[1], L. Pang[4], M. Hehn[2], S. Alebrand[3], M. Cinchetti[3], G. Malinowski[2,5], Y. Fainman[4], M. Aeschlimann[3] and E. E. Fullerton[1,4*]

The possibility of manipulating magnetic systems without applied magnetic fields have attracted growing attention over the past fifteen years. The low-power manipulation of the magnetization, preferably at ultrashort timescales, has become a fundamental challenge with implications for future magnetic information memory and storage technologies. Here we explore the optical manipulation of the magnetization in engineered magnetic materials. We demonstrate that all-optical helicity-dependent switching (AO-HDS) can be observed not only in selected rare earth–transition metal (RE–TM) alloy films but also in a much broader variety of materials, including RE–TM alloys, multilayers and heterostructures. We further show that RE-free Co–Ir-based synthetic ferrimagnetic heterostructures designed to mimic the magnetic properties of RE–TM alloys also exhibit AO-HDS. These results challenge present theories of AO-HDS and provide a pathway to engineering materials for future applications based on all-optical control of magnetic order.

The manipulation of the magnetization of magnetic systems without resorting to applied magnetic fields is attractive for potential information and memory storage device applications. Examples include the demonstration of spin-transfer-torque switching[1], the emerging potential of electric fields to manipulate magnetic devices[2] and magnetization switching using femto- or picosecond pulsed lasers[3–5]. Here we explore optical manipulation of the magnetization of engineered magnetic materials and devices. We demonstrate that AO-HDS can be observed not only in selected RE–TM alloy films[3–5] but also in a much broader variety of materials, including alloys, multilayers, heterostructures and RE-free Co–Ir-based synthetic ferrimagnets (SFIs) as shown schematically in Fig. 1.

The discovery of AO-HDS in RE-free TM-based heterostructures may enable breakthroughs for numerous applications because it exploits materials that are employed at present in magnetic data storage, memories and logic technologies. Moreover, by systematically studying a range of materials displaying AO-HDS, we gain valuable insight into the underlying mechanisms involved. Indeed, the common denominator of the diverse structures in Fig. 1 showing AO-HDS is that they consist of two antiferromagnetically coupled magnetic sublattices exhibiting magnetization compensation (and therefore angular momentum compensation) at temperatures near or above room temperature. Our results highlight that compensation plays a major role and that this compensation can be established at the atomic level as in alloys but also over a larger nanometre scale in multilayers or heterostructures. Femtosecond laser pulses are 1,000–10,000 times shorter than the shortest magnetic fields pulses[6] or spin-polarized current pulses[7] needed to induce magnetization reversal. Moreover, this process is also considerably more energy efficient; an energy lower than 10 fJ is expected to be sufficient to switch a $20 \times 20\,nm^2$ area of magnetic material[8]. However, up to now observations of AO-HDS are only reported for a narrow composition range of the following amorphous RE–TM ferrimagnetic alloy films of GdFeCo (ref. 3), TbCo (ref. 4) and TbFe (ref. 9).

Here we report optical responses for four classes of magnetic thin-film materials exhibiting perpendicular magnetic anisotropy (PMA) and demonstrate AO-HDS: RE–TM alloys (Fig. 1a); RE/TM multilayers (Fig. 1b); coupled RE–TM heterostructures (Fig. 1c); and SFIs that are made of antiferromagnetically coupled TM-based ferromagnetic layers that mimic a RE–TM ferrimagnetic material (Fig. 1d). For the purpose of this Article we categorize the responses after sweeping the laser beam over the sample as falling into either one of two general categories: thermal demagnetization (Fig. 2a) or AO-HDS (Fig. 2b). Thermal demagnetization is characterized by the formation of magnetic domains with random up or down orientation, that form independent of the laser beam helicity, whereas AO-HDS describes deterministic magnetization reversal of the material under the beam with no external magnetic field. In that case the orientation of the magnetization after the laser has passed depends on the helicity of the laser as shown in Fig. 2b. There are samples at the boundary between these two behaviours that exhibit a mixed behaviour (highlighted in Supplementary Fig. 1).

We have explored the response in more than 400 separate samples that span a range of fundamental magnetic properties such as spin–orbit coupling, exchange coupling, magnetization and magnetocrystalline anisotropy. This study greatly broadens the range of materials showing AO-HDS and highlights a pathway for engineering materials for optical control using exchange-coupled heterostructures based on ferromagnetic layers such as Co, [Co/Pt] and [Co/Ni] that have found broad application in magnetic nanotechnologies[10–13].

So far, the reports of AO-HDS have exclusively focused on RE–TM alloy films and many of the proposed mechanisms are linked to the unique properties of these alloys. The magnetism

[1]Center for Magnetic Recording Research, University of California San Diego, La Jolla, California 92093-0401, USA, [2]Institut Jean Lamour, UMR CNRS 7198 – Université de Lorraine – boulevard des aiguillettes, BP 70239, Vandoeuvre cedex F-54506, France, [3]Department of Physics and Research Center OPTIMAS University of Kaiserslautern, Erwin Schroedinger Str. 46, Kaiserslautern D-67663, Germany, [4]Department of Electrical and Computer Engineering, University of California San Diego, La Jolla, California 92093-0401, USA, [5]Laboratoire de Physique des Solides, Université Paris-Sud, CNRS UMR 8502, Orsay 91405, France. *e-mail: stephane.mangin@univ-lorraine.fr; efullerton@ucsd.edu

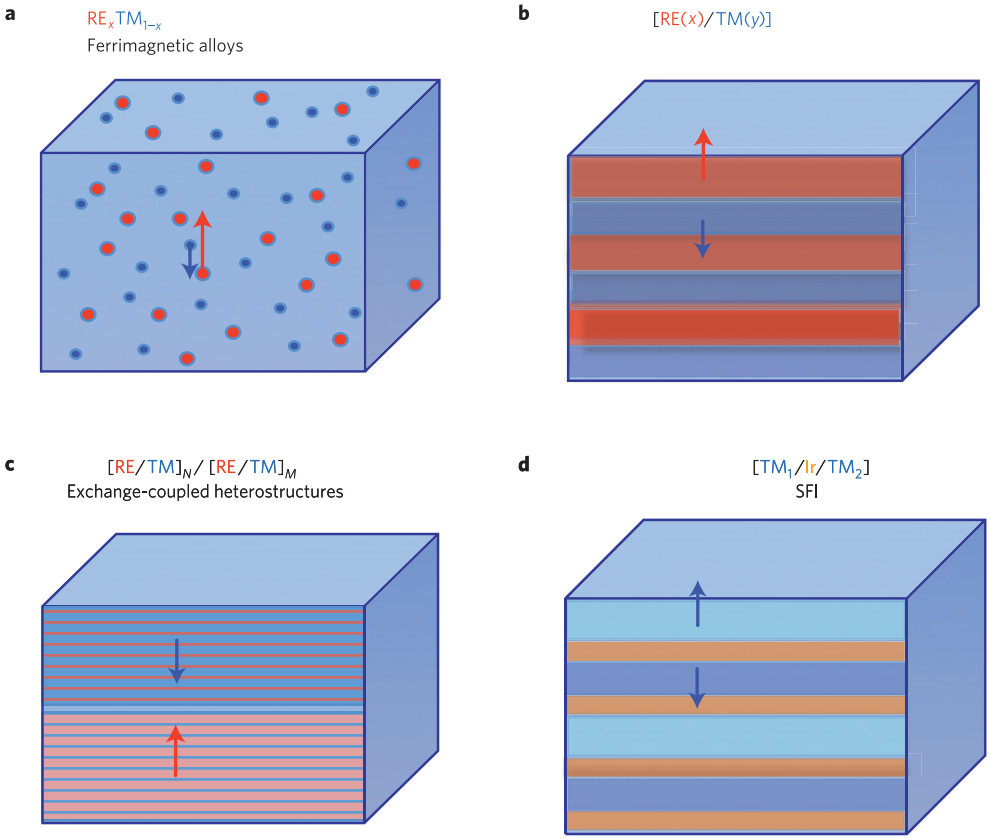

Figure 1 | Schematic of the four types of ferromagnetic sample that have been studied and exhibit AO-HDS. a, Thin-film RE–TM alloys. **b**, $[RE/TM]_N$ multilayers. **c**, Exchange-coupled $[RE/TM]_N/[RE/TM]_M$ heterostructures. **d**, SFI made of two TM layers antiferromagnetically coupled through 0.4 nm Ir interlayers. Each type of magnetic structure has shown either AO-HDS or thermal demagnetization depending on the thickness, layer structure and/or atomic concentration of the sample.

of the 14 RE elements comes primarily from the partially filled 4*f* band. In RE–TM alloys the net magnetization results from the magnetization of the RE and TM sublattices. In the case of the light RE (4*f* electrons <7) the two sublattices are exchange-coupled ferromagnetically whereas for heavy RE (4*f* electrons ≥ 7) the two sublattices are exchange-coupled antiferromagnetically, forming a ferrimagnet. Depending on the concentration and temperature, the net magnetization of the alloy can be along either the RE or TM magnetization sublattice[14,15]. As a result of the high Curie temperature (T_C) of TMs such as Fe and Co compared with the RE elements, the RE sublattice magnetization has a stronger temperature dependence and the T_C of the alloys decreases with increasing RE content. This results in a narrow composition range where the two sublattice magnetizations compensate at a given temperature (T_{Mcomp}), resulting in a net magnetization equal to zero. For temperatures below T_{Mcomp} the net magnetization is parallel to the RE moments whereas above it the net magnetization is parallel to the TM moments. Because the Landé factor of the RE is smaller than the one of the TM the angular momentum compensation temperature (T_{Lcomp}) is higher than T_{Mcomp}. The concentration range for which compensation exists is rather limited (~20–30 at.% RE).

Amorphous RE–TM alloys

We have investigated a range of RE–TM alloys, RE = Gd, Tb, Dy and Ho and TM = Fe, Co or Fe–Co alloys to study the influence of the RE type and concentration on the AO-HDS. (Previous studies of Gd–TM alloys are given in refs 3,5,16–18 and Tb–TM alloys in refs 4,9.) These compounds all form amorphous ferrimagnetic alloys but exhibit a wide range of magnetic parameters such as the exchange coupling, spin–orbit coupling, magnetocrystalline anisotropy, magnetization and compensation temperatures[14,15]. For instance, Gd has a half-filled 4*f* shell resulting in a net orbital moment of zero. The spin–orbit coupling (and the coupling of the Gd moment to the lattice) is very weak in Gd-based alloys, leading to low magnetocrystalline anisotropy. However, for Tb, Dy and Ho the presence of a large orbital momentum leads to a strong spin–orbit coupling and larger magnetic anisotropy. The large difference in spin–orbit coupling in the different RE materials has been shown to have a significant influence on the demagnetization processes in response to ultrafast laser pulses[19].

Four different types of alloy have been grown: Gd_xFeCo_{1-x}, Tb_xCo_{1-x}, Dy_xCo_{1-x} and Ho_xFeCo_{1-x}. Each was deposited on a glass/Ta(4 nm) substrate and capped with a 4 nm Ta layer. Most of the alloy samples show strong PMA. Only Gd_xFeCo_{1-x} alloys with $x<22\%$ and $x>28\%$ showed in-plane remanent magnetization due to low magnetocrystalline anisotropy and increasing magnetization as we move away from the compensation point. In Fig. 3 we identify as a function of average composition for which samples we observe thermal demagnetization or AO-HDS (or in-plane magnetization for Gd-based alloys). We observe AO-HDS for all of the ferrimagnetic alloys studied, regardless of the specific RE element, indicating that this is a general response for this class of materials. However, we observe AO-HDS for only a narrow window of RE concentrations around 25%, in agreement with previous studies[4,9]. For different samples we can determine whether T_{Mcomp} is above or below room temperature by measuring both the symmetry of the magneto-optic Kerr effect (MOKE) hysteresis loops and the dependence of the coercive field with average composition. The

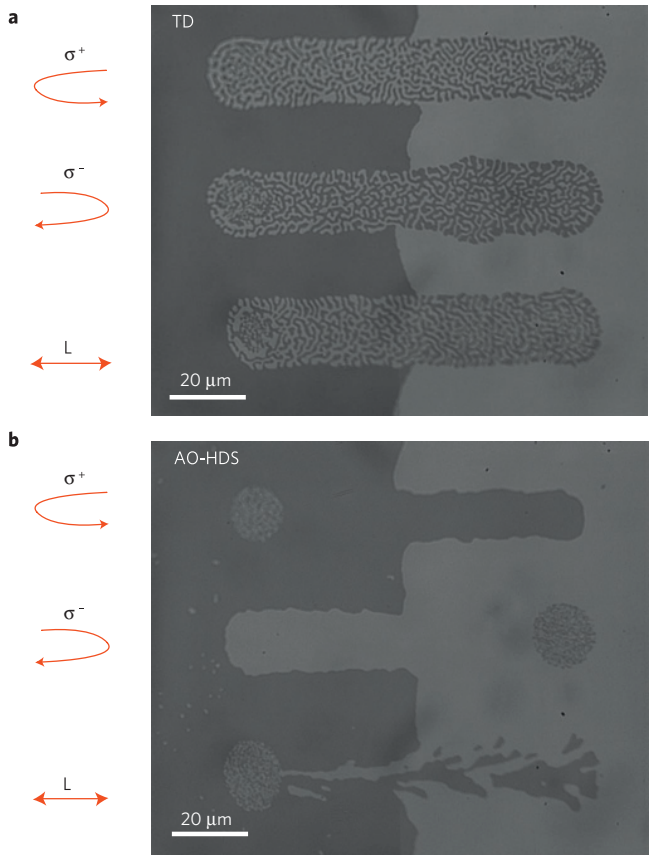

Figure 2 | Examples of the two optical responses for two different samples. a,**b**, $[Co(0.8\,nm)/Tb(0.4\,nm)]_{\times 21}$ multilayers showing thermal demagnetization (TD, **a**) and $[Co(0.5\,nm)/Tb(0.4\,nm)]_{\times 28}$ multilayers showing AO-HDS (**b**). For each sample, three types of polarized laser beam were swept over the sample and the magnetization pattern was subsequently imaged: from top to bottom, right circularly polarized light (σ^+), left circularly polarized light (σ^-) and linearly polarized light (L). In the images, dark contrast corresponds to one orientation of magnetization and light contrast the opposite.

MOKE response measures primarily the TM sublattice. Therefore for samples where T_{Mcomp} is below room temperature and the net magnetization is parallel to the TM moments the MOKE hysteresis loop will have the same symmetry as a ferromagnetic samples. However when T_{Mcomp} is above room temperature and the net magnetization is parallel to the RE moments the MOKE hysteresis loop will appear inverted. When $T = T_{Mcomp}$ the net magnetization goes to zero and the coercive field diverges. Thus plotting the coercive field versus composition a peak in the coercive field occurs when T_{Mcomp} approaches room temperature. In Supplementary Fig. 2 we show the evolution of the coercive field for each alloy composition. In Fig. 3 we highlight compositions where the T_{Mcomp} is below room temperature (blue region). Figure 3 clearly indicates that most alloys exhibiting AO-HDS behaviour show T_{Mcomp} near or above room temperature. This behaviour is in agreement with recent results shown for GdFeCo alloys[20].

RE–TM multilayers

To investigate the role of the atomic ordering and consequently the exchange coupling between the two sublattices on AO-HDS, we extended these studies to RE–TM multilayers. By evolving from an alloy to a well-defined layered structure we are tuning the heterogeneity of the system. Indeed it was recently shown that the demagnetization behaviour can be quite different in alloys compared with multilayer structures, as shown by comparing FeNi alloy[21] and Fe/Ni multilayer films[22]. Moreover, there is emerging evidence that laser-induced superdiffusive spin currents can flow in heterogeneous systems (for example, refs 23–25) that may play a role in the demagnetization process and AO-HDS.

The systems we studied are $[RE(t_1)/TM(t_2)]_N$ multilayers, where N is the number of repeats. Each multilayer was grown on a glass/Ta(4 nm) substrate and subsequently covered with Ta(4 nm). The total multilayer thickness was kept constant at ∼25 nm to be comparable to the alloy films. In these structures it is possible to tune the average composition or to keep the RE–TM ratio constant and grow different structures starting from a homogeneous isotropic amorphous alloy to well-defined multilayers (Fig. 4). The sample heterogeneity is tuned by increasing the layer thicknesses and reducing N to keep a constant total thickness and average concentration. In all cases the magnetization of the RE layers is antiferromagnetically coupled to that of the TM layers.

For [Gd/Co] multilayers, once the Gd layer thickness exceeds 1 nm the PMA becomes too weak and the magnetization lies in-plane. However, for [Tb/Co] and [Ho/CoFe] multilayers, a strong PMA and a T_C larger than room temperature are measured even for a 6 nm periodicity (that is 3 nm layers). An example is shown in Fig. 4 where we compare three samples with the same average composition and total thickness: an $Tb_{26}Co_{74}$ (25 nm) alloy, $[Tb(0.3\,nm)/Co(0.3\,nm)]_{\times 42}$ and $[Tb(2.5\,nm)/Co(2.5\,nm)]_{\times 5}$ multilayers. X-ray reflectivity measurements performed on [Co/Tb] multilayers (Supplementary Fig. 3) show clear super-structure peaks confirming the distinct layers and periodic nature of the multilayer samples. As can be seen in Fig. 4, AO-HDS can be observed in all three samples and these measurements represent the first observation of AO-HDS in multilayer structures.

From Fig. 4, it is clear that AO-HDS is not limited to amorphous alloys. The multilayer systems show similar compensation effects as the alloys and T_{Mcomp} can be defined from the sign change of the magneto-optic Kerr effect signal and the divergence of the coercivity (for example, Fig. 3 and Supplementary Fig. 4). In Fig. 3 we give a synopsis of the data similar to the one shown for the alloys to summarize a set of multilayer samples where the RE thickness ranged from 0.3 to 0.5 nm and the TM thickness ranged from 0.25 to 1.0 nm. For simplicity, the data are gathered as a function of the average composition (although some care is needed in making such a plot as T_{Mcomp} for a given average composition depends on the repeat period and tends to decrease with increasing layer thickness). Indeed, only a narrow set of average composition exhibit AO-HDS and most samples showing AO-HDS have compensation temperatures near or above room temperature. These results suggest that not only does the magnetic compensation play a major role for the AO-HDS process but, crucially, that magnetic compensation does not have to be established at the atomic level but can be obtained while averaging over larger length scales of at least 6 nm (Fig. 4). This upper limit in the multilayers is set by the layer thicknesses that maintain PMA.

RE–TM multilayer heterostructures

For the multilayers described above the response to optical excitations seems to be controlled by the average magnetic properties. To further probe this averaging process we formed exchange-coupled stacks (Fig. 1c) composed of two types of multilayer such as $[Tb(0.5\,nm)/Co(0.45\,nm)]_N$ and $[Tb(0.35\,nm)/Co(0.7\,nm)]_{25-N}$. $[Tb(0.5\,nm)/Co(0.45\,nm)]_{25}$ multilayer samples have a T_{Mcomp} around 450 K and the net magnetization at room temperature is aligned with the RE sublattice. These multilayers show AO-HDS. Conversely, for the $[Tb(0.35\,nm)/Co(0.7\,nm)]_{25}$ multilayers the net magnetization is parallel to the TM layers and therefore does not exhibit a magnetic compensation temperature at any temperature above room temperature. As shown schematic-

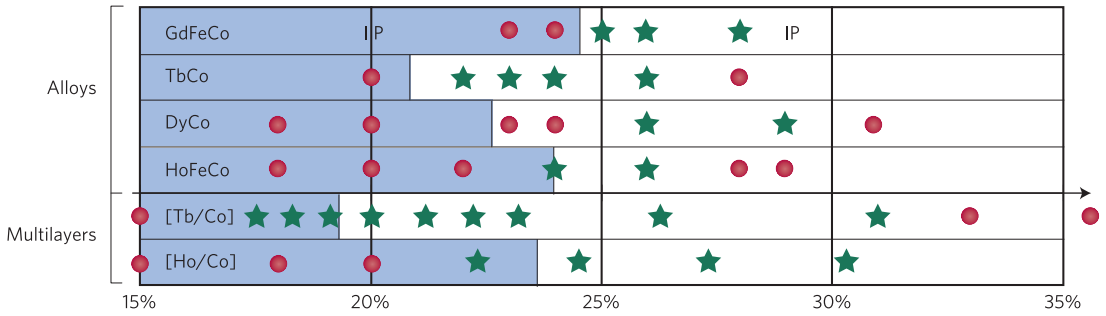

Figure 3 | Response to optical excitation for RE–TM alloys (Gd_xFeCo_{1-x}, Tb_xCo_{1-x}, Dy_xCo_{1-x}, Ho_xFeCo_{1-x}) and two types of RE–TM multilayer ([Tb/Co] and [Ho/CoFe]) as a function of the RE concentration (x). Red dots indicate thermal demagnetization and green stars AO-HDS. All of these alloys show perpendicular anisotropy except the two GdFeCo alloys marked IP (for in-plane anisotropy). The shaded regions correspond to alloy compositions for which T_{Mcomp} is below room temperature. For the multilayers the RE layer thicknesses varied from 0.3 to 0.5 nm and the TM layers varied from 0.25 to 1.0 nm.

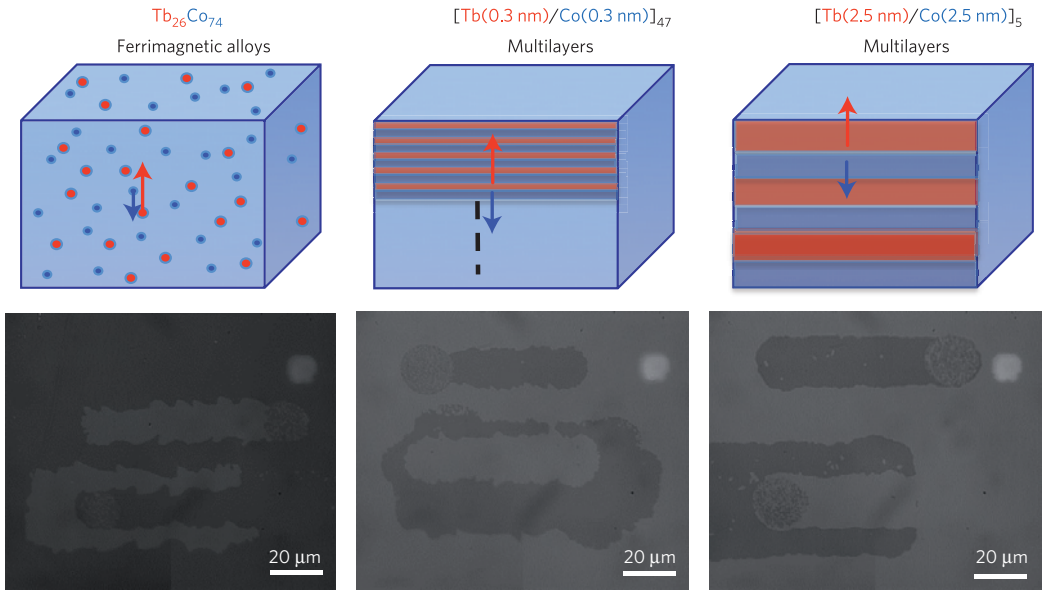

Figure 4 | Samples swept with circularly polarized beams (σ^+ or σ^-). All-optical switching can be observed for three different samples: a $Tb_{26}Co_{74}$ alloy, a $[Tb(0.3\,nm)/Co(0.3\,nm)]_{\times 42}$ multilayer and a $[Tb(2.5\,nm)/Co(2.5\,nm)]_{\times 5}$ multilayer, which have the same average concentration of Tb and Co atoms.

ally in Fig. 1c, the composite structure will be a mix of these two behaviours and the compensation composition will be given by the average of the total film structure. $[Tb(0.5\,nm)/Co(0.45\,nm)]_N/[Tb(0.35\,nm)/Co(0.7\,nm)]_{25-N}$ heterostructures were studied as a function of N. For $N = 25 - 15$ AO-HDS was observed, whereas for $N < 15$ thermal demagnetization is observed. This transition happens as the T_{Mcomp} of the average film structure is found to cross room temperature (Supplementary Fig. 5a); that is, when T_{Mcomp} less than room temperature no AO-HDS is observed. A similar behaviour is obtained from another set of heterostructures, $[Tb(0.5\,nm)/Co(0.45\,nm)]_N$,/$[Tb(0.35\,nm)/Co(0.53\,nm)]_{25-N}$, where again the onset of AO-HDS is linked to the transition of T_{Mcomp} of the average film structure with room temperature (Supplementary Fig. 5b).

SFI heterostructures

From the results shown above, we observe AO-HDS for a broad range of ferrimagnetic RE–TM structures and compositions with the following average magnetic properties: the samples exhibit PMA; the samples consist of two distinct magnetic sublattices (or layers) that are antiferromagnetically coupled; and the two magnetic sublattices have different temperature dependences such that compensation of the average magnetization is present near or above room temperature.

A crucial question is whether a RE-free heterostructure that exhibits these magnetic characteristics will also exhibit AO-HDS. To address this, we synthesized SFI based on Co/Ir multilayers. Previous studies have shown that Co–Ir multilayers possess the combination of PMA and strong antiferromagnetic interlayer coupling to form a synthetic antiferromagnet[26,27]. In the present structure, the Ir layer thickness of 0.4 nm was chosen to maximize the antiferromagnetic coupling between the ferromagnetic layers. We initially formed antiferromagnetically coupled structures $[Co(1\,nm)/Ir/Co(0.8\,nm)/Ir]_N$. These structures exhibited PMA and ferrimagnetic properties but we were not able to observe AO-HDS. We either were not able to image domains or only observe thermal demagnetization effects. However, because the 1 nm Co layer has both a higher moment and higher T_C than the 0.8 nm layer this structure does not exhibit a T_{Mcomp} and thus only fulfils the first two magnetic properties listed above.

To design a SFI structure that exhibits a T_{Mcomp} we replace the 0.8 nm Co layer with a $Co(0.4\,nm)/Ni(0.6\,nm)/Pt(t_2)/Co(0.4\,nm)$ magnetic layer structure where the Pt layer could be adjusted to control the total moment and exchange and therefore the

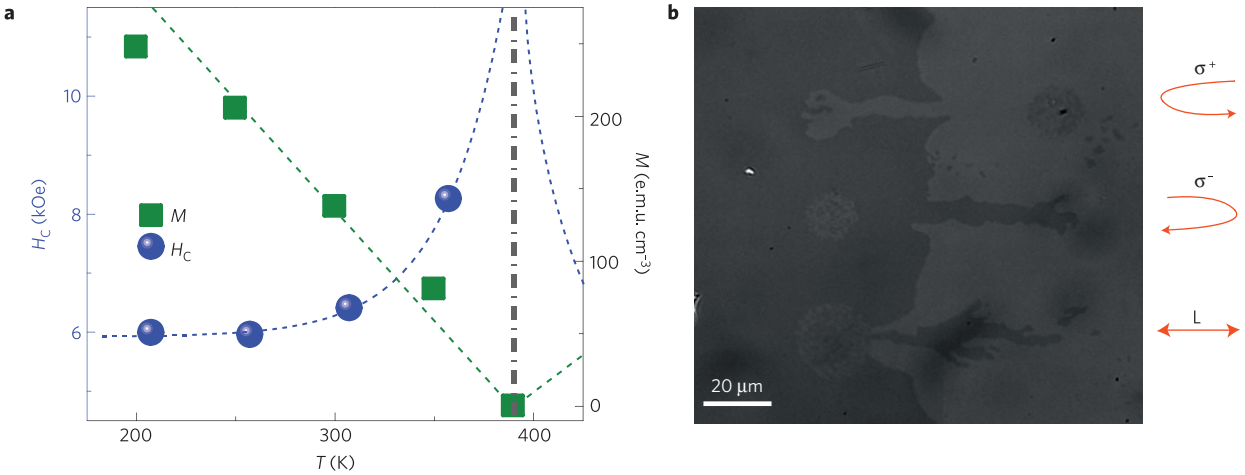

Figure 5 | Magnetic measurements of a Ta(4 nm)/Pd(3 nm)/[Co(1 nm)/Ir/Co(0.4 nm)/Ni(0.6 nm)/Pt(0.3 nm)/Co(0.4 nm)/Ir]5/Pd(3 nm) SFI structure. **a**, Remanent magnetization M and coercive field H_C as a function of temperature allow us to define a compensation temperature at $T_{Mcomp} = 380$ K. **b**, Images after scanning the laser with three types of polarized beam that were swept over the sample: from top to bottom, right circularly polarized light (σ^+), left circularly polarized light (σ^-) and linearly polarized light (L).

Curie temperature of the composite layer. This resulted in the following Co/Ir/CoNiPtCo/Ir heterostructures: Ta(4 nm)/Pd(3 nm)/[Co(t_1)/Ir/CoNiPt(t_2)Co/Ir]$_N$/Pd(3 nm). This structure has PMA and at room temperature a field of 10 T is not sufficient to overcome the antiferromagnetic exchange coupling (Supplementary Fig. 6). The thicknesses of t_1 and t_2 can be chosen such that at room temperature the CoNiPtCo composite layer total magnetization is larger than the Co layer but has a lower Curie temperature compared with the Co layer with thickness t_2. Consequently, the CoNiPtCo layer moment decreases faster than that of the Co layer with increasing temperature, resulting in a magnetic compensation temperature for selected structures. By tuning the layer thickness of the CoNiPtCo composite structure we were able to tune T_{Mcomp} and successfully synthesize SFI systems, showing the three properties described above.

Figure 5a shows the temperature dependence of the magnetization and coercive fields of a Ta(4 nm)/Pd(3 nm)/[Co(1 nm)/Ir/Co(0.4 nm)/Ni(0.6 nm)/Pt(0.3 nm)/Co(0.4 nm)/Ir]$_5$/Pd(3 nm) SFI structure. The divergence of H_C correlated to the decrease of the net magnetization to zero determines $T_{Mcomp} = 380$ K. The compensation temperature may be tuned by adjusting the layer thicknesses in the composite structure. For instance, changing the Pt layer to 0.6 nm in the CoNiPtCo layer decreases T_{Mcomp} to 300 K (Supplementary Fig. 7). Most importantly, as shown in Fig. 5b, the SFI structures with T_{Mcomp} greater than room temperature exhibit AO-HDS, demonstrating control of the sublattice magnetization with light.

The possibility of using engineered material based solely on TM structures such as Co and CoNiPtCo layers for AO-HDS greatly expands the potential for future technological applications. Indeed, those materials are compatible with magnetic recording and magnetoresistive random-access memory technologies. Reducing the lateral size of the laser spot and demonstrating AO-HDS for nanosize elements is the next step. Note that the magnetic data storage industry has already demonstrated heat-assisted magnetic recording where near-field optical tranducers are used to focus a laser beam to sub-100 nm spots to enable writing of high-anisotropy magnetic recording media that cannot be written solely by magnetic fields[28].

Beyond providing a pathway to engineering materials for future applications, our study also probes the fundamental microscopic mechanisms behind AO-HDS. Different models have been discussed in several recent papers and review articles[3–5,17,20,29,30]. The most discussed models are based on either the existence of an effective field created by the circular polarized light through the inverse Faraday effect, the transfer of angular momentum from the light to the magnetic system or, most recently, on the formation of a transient ferromagnetic state due to different demagnetization times for RE and TM sublattices. In this last model the light helicity plays a secondary role, through a helicity dependence of the absorption. In the context of this model, spin–orbit coupling is assumed to have a large impact on the AO-HDS properties because it significantly alters the ultrafast demagnetization processes[19,31].

In the present experiments, we observed AO-HDS involving materials showing T_C ranging from near room temperature ($Ho_{26}CoFe_{74}$) to more than 500 K ($Gd_{25}CoFe_{75}$). The change in T_C that is directly related to exchange coupling strength in the considered material does not seem to be a determining parameter for AO-HDS. Moreover, the character of the exchange coupling is strongly modified going from an alloy to a multilayer but AO-HDS still persists. In the SFI systems, the two antiferromagnetically coupled layers are made of TMs, meaning that the presence of a RE (and, hence, a slow demagnetization time[32]) does not seem to be a necessary condition for AO-HDS. Further, our study shows that AO-HDS may be observed for materials with low spin–orbit coupling such as GdFeCo, but also high spin–orbit coupling such as TbCo, DyCo and CoPt. The fact that multilayers, heterostructures and SFI systems show AO-HDS suggests that the explanation cannot be limited to two-atom models involving a core-level RE moment antiferromagnetically coupled to a TM moment. Finally, the results do not seem to be particularly sensitive to the microstructure of the samples, suggesting that superdiffusive currents are also not a necessary condition for AO-HDS.

Our measurements and our observation of AO-HDS in RE-free SFI heterostructures suggest that the underlying mechanism for this phenomenon is closely linked to the existence of a magnetic compensation state. In this context, a model based on the transfer of both angular momentum and heat from the light to the sample would most easily explain our data. Light would transfer heat so that the temperature for which the total needed angular momentum exchange is small can be reached; then the angular momentum transfer from the light to the sample would be sufficient to induce magnetization switching. That would explain why a limited number of samples having

T_{Mcomp} slightly smaller than room temperature have shown AO-HDS as well. Indeed, the essential parameter is probably not the magnetization compensation (at T_{Mcomp}) but the angular momentum compensation, which is at slightly higher temperatures for RE–TM alloys. A recent phenomenological two-sublattice model[33] that distinguishes magnetization changes of relativistic and exchange origin predicts that in the exchange-dominated regime sublattices can show highly counterintuitive transitions between parallel and antiparallel alignment. Such a general model[34,35] may also provide a framework to understand our results.

In conclusion, we have demonstrated AO-HDS for a range of engineered materials such as RE–TM alloys, multilayers and heterostructures involving different types of magnetic element. The common denominator of the diverse RE–TM structures showing AO-HDS is two ferrimagnetic sublattices showing distinct temperature dependences that can be magnetically compensated at a selected temperature. We have also shown that RE-free heterostructures that mimic the properties of RE–TM alloys also exhibit AO-HDS. These results offer valuable information to help us understand the underlying fundamental mechanisms involved. More importantly, these findings open a route for designing complex materials using well-known techniques with which magnetization can be controlled by the application of light.

Methods

We used optical pulses that had a central wavelength of 800 nm (1.55 eV), a pulse duration of about 100 fs at the sample position and a repetition rate of 0.1–1 kHz. A schematic of the optical test facilities where AO-HDS measurements were performed is shown in Supplementary Fig. 8. The response of the magnetic film was studied using a static Faraday microscope to image the magnetic domains while the laser is illuminating the sample. The helicity of the beam is controlled by a zero-order quarter-wave plate, which transforms linearly polarized light (L) into circularly left- (σ^+) or right-polarized light (σ^-). The present measurements are performed at room temperature and the laser beam was swept at a constant rate of $\sim$3–20 $\mu m\,s^{-1}$ with the typical laser spot size of $\sim$80 μm. The laser power was adjusted to achieve either thermal demagnetization or AO-HDS and varied from sample to sample (see Supplementary Fig. 9 for an example). Typical laser powers for 1 kHz repetition rates are 0.5–2 μW. The threshold power scales with the repetition rate, indicating it is the energy/pulse that determines the threshold power. For the film thicknesses used in this study, roughly 35% of the laser power is absorbed by the film.

All of the samples were grown by d.c. magnetron sputtering from elemental sources onto room-temperature glass substrates. Alloys were grown by co-sputtering where the source powers controlled the composition. Multilayers and heterostructures were formed by sequential deposition of layers. Magnetic moment and hysteresis measurements were performed using a vibrating sample magnetometer and magneto-optic Kerr effect measurements. Sample structures were characterized by X-ray reflectivity.

Received 22 June 2013; accepted 13 December 2013; published online 16 February 2014

References

1. Katine, J., Albert, F. J., Buhrman, R. A., Myers, E. B. & Ralph, D. C. Current-driven magnetization reversal and spin-wave excitations in Co/Cu/Co pillars. *Phys. Rev. Lett.* **84,** 3149–3152 (2000).
2. Ohno, H. *et al.* Electric-field control of ferromagnetism. *Nature* **408,** 944–946 (2000).
3. Stanciu, C. D. *et al.* All-optical magnetic recording with circularly polarized light. *Phys. Rev. Lett.* **99,** 047601 (2007).
4. Alebrand, S. *et al.* Light-induced magnetization reversal of high-anisotropy TbCo alloy films. *Appl. Phys. Lett.* **101,** 162408 (2012).
5. Kirilyuk, A., Kimel, A. V. & Rasing, T. Laser-induced magnetization dynamics and reversal in ferrimagnetic alloys. *Rep. Prog. Phys.* **76,** 026501 (2013).
6. Tudosa, I. *et al.* The ultimate speed of magnetic switching in granular recording media. *Nature* **428,** 831–833 (2004).
7. Bedau, D. *et al.* Ultrafast spin-transfer switching in spin valve nanopillars with perpendicular anisotropy. *Appl. Phys. Lett.* **96,** 022514 (2010).
8. Savoini, M. *et al.* Highly efficient all-optical switching of magnetization in GdFeCo microstructures by interference-enhanced absorption of light. *Phys. Rev. B* **86,** 140404(R) (2012).
9. Hassdenteufel, A. *et al.* Thermally assisted all-optical helicity dependent magnetic switching in amorphous $Fe_{100-x}Tb_x$ alloy films. *Adv. Mater.* **25,** 3122–3128 (2013).
10. Lambert, C. H. *et al.* Quantifying perpendicular magnetic anisotropy at the Fe–MgO(001) interface. *Appl. Phys. Lett.* **102,** 122410 (2013).
11. Zeper, W. B., Greidanus, F. J. A. M., Carcia, P. F. & Fincher, C. R. Perpendicular magnetic anisotropy and magneto-optical Kerr effect of vapor-deposited Co/Pt-layered structures. *J. Appl. Phys.* **65,** 4971–4975 (1989).
12. Girod, S. *et al.* Strong perpendicular magnetic anisotropy in Ni/Co(111) single crystal superlattices. *Appl Phys. Lett.* **94,** 262504 (2009).
13. Mangin, S. *et al.* Current-induced magnetization reversal in nanopillars with perpendicular anisotropy. *Nature Mater.* **5,** 210–215 (2006).
14. Hansen, P., Clausen, C., Much, G., Rosenkranz, M. & Witter, K. Magnetic and magneto-optical properties of rare-earth transition-metal alloys containing Gd, Tb, Fe, Co. *J. Appl. Phys.* **66,** 756–767 (1989).
15. Hansen, P., Klahn, S., Clausen, C., Much, G. & Witter, K. Magnetic and magneto-optical properties of rare-earth transition-metal alloys containing Dy, Ho, Fe, Co. *J. Appl. Phys.* **69,** 3194–3207 (1991).
16. Steil, D., Alebrand, S., Hassdenteufel, A., Cinchetti, M. & Aeschlimann, M. All-optical magnetization recording by tailoring optical excitation parameters. *Phys. Rev. B* **84,** 224408 (2011).
17. Vahaplar, K. *et al.* All-optical magnetization reversal by circularly polarized laser pulses: Experiment and multiscale modeling. *Phys. Rev. B* **85,** 104402 (2012).
18. Alebrand, S., Steil, D., Hassdenteufel, A., Cinchetti, M. & Aeschlimann, M. Interplay of heating and helicity in all-optical magnetization switching. *Phys. Rev. B* **85,** 092401 (2012).
19. Khorsand, A. R. *et al.* Element-specific probing of ultrafast spin dynamics in multisublattice magnets with visible light. *Phys. Rev. Lett.* **110,** 107205 (2013).
20. Medapalli, R. *et al.* The role of magnetization compensation point for efficient ultrafast control of magnetization in $Gd_{24}Fe_{66.5}Co_{9.5}$ alloy. *Eur. Phys. J. B* **86,** 183 (2013).
21. Mathias, S. *et al.* Probing the timescale of the exchange interaction in a ferromagnetic alloy. *Proc. Natl Acad. Sci. USA* **109,** 4792–4797 (2012).
22. Rudolf, D. *et al.* Ultrafast magnetization enhancement in metallic multilayers driven by superdiffusive spin current. *Nature Commun.* **3,** 1037 (2012).
23. Battiato, M., Carva, K. & Oppeneer, P. M. Superdiffusive spin transport as a mechanism of ultrafast demagnetization. *Phys. Rev. Lett.* **105,** 027203 (2010).
24. Graves, C. E. *et al.* Nanoscale spin reversal by non-local angular momentum transfer following ultrafast laser excitation in ferrimagnetic GdFeCo. *Nature Mater.* **12,** 293–298 (2013).
25. Turgut, E. *et al.* Controlling the competition between optically induced ultrafast spin-flip scattering and spin transport in magnetic multilayers. *Phys. Rev. Lett.* **110,** 197201 (2013).
26. Den Broeder, F. J. A., Hoving, W. & Bloemen, P. J. H. Magnetic anisotropy of multilayers. *J. Magn. Magn. Mater.* **93,** 562–570 (1991).
27. Itoh, H., Yanagihara, H., Suzuki, K. & Kita, E. Coexistence of the uniaxial anisotropy and the antiferromagnetic coupling in Co/Ir(111) superlattices. *J. Magn. Magn. Mater.* **257,** 184–189 (2003).
28. Stipe, B. C. *et al.* Magnetic recording at 1.5 $Pb\,m^{-2}$ using an integrated plasmonic antenna. *Nature Photon.* **4,** 484–488 (2010).
29. Kirilyuk, A., Kimel, A. & Rasing, Th. Ultrafast optical manipulation of magnetic order. *Rev. Mod. Phys.* **82,** 2731–2784 (2010).
30. Ostler, T. A. *et al.* Ultrafast heating as a sufficient stimulus for magnetization reversal in a ferrimagnet. *Nature Commun.* **3,** 666 (2012).
31. Koopmans, B. *et al.* Explaining the paradoxical diversity of ultrafast laser-induced demagnetization. *Nature Mater.* **9,** 259–265 (2009).
32. Radu, I. *et al.* Transient ferromagnetic-like state mediating ultrafast reversal of antiferromagnetically coupled spins. *Nature* **472,** 205–208 (2011).
33. Mentink, J. H. *et al.* Ultrafast spin dynamics in multisublattice magnets. *Phys. Rev. Lett.* **108,** 057202 (2012).
34. Schellekens, A. J. & Koopmans, B. Microscopic model for ultrafast magnetization dynamics of multisublattice magnets. *Phys. Rev. B* **87,** 020407 (2013).
35. Wienholdt, S., Hinzke, D., Carva, K., Oppeneer, P. M. & Nowak, U. Orbital-resolved spin model for thermal magnetization switching in rare-earth-based ferrimagnets. *Phys. Rev. B* **88,** 020406 (2013).

Acknowledgements

We would like to thank M. Fuhrman and R. Tolley for technical assistance with optical measurements and fruitful discussion, and J. M. Dubois for his constant support. This

work was supported by the ANR, ANR-10-BLANC-1005 'Friends', and work at UCSD was partially supported by a grant from the Advanced Storage Technology Consortium and the Office of Naval Research (ONR) MURI programme. It was also supported by The Partner University Fund 'Novel Magnetic Materials for Spin Torque Physics' as well as the European Project (OP2M FP7-IOF-2011-298060) and the Region Lorraine. V.U. was supported by DOE, Office of Basic Energy Sciences award #DE-SC0003678.

Author contributions

S.M., M.H., Y.F., M.A. and E.E.F. designed and coordinated the project; M.G., C-H.L., M.H., G.M. and S.M. grew, characterized and optimized the samples. C-H.L., D.S., L.P., S.A., V.U., M.C. and S.M. built and operated the Kerr microscope and the pump laser set-up. S.M. and E.E.F. coordinated work on the paper with contributions from D.S., M.H., S.A., M.C., M.A. and regular discussions with all authors.

Additional information

Supplementary information is available in the online version of the paper. Reprints and permissions information is available online at www.nature.com/reprints. Correspondence and requests for materials should be addressed to S.M. or E.E.F.

Competing financial interests

The authors declare no competing financial interests.